The Journal of Experimental Biology 201, 2359–2366 (1998)
Printed in Great Britain © The Company of Biologists Limited 1998
JEB1426

AUGMENTED RESPIRATION IN A FLYING INSECT

YUTAKA KOMAI*

ERATO, Kawachi Millibioflight Project, Park Building, 4-7-6 Komaba, Meguro, Tokyo, Japan

*Present address: Department of System Design Engineering, Keio University, 3-14-1, Hiyoshi, Kohoku-ku, Yokohama, Kanagawa, 223, Japan (e-mail: miesha@tani.sd.keio.ac.jp)

Accepted 4 June; published on WWW 27 July 1998

Summary

The properties of the gas transport system in a tethered flying insect were investigated by directly measuring the oxygen partial pressure (P_{O_2}) in a wing muscle of the sweet potato hawkmoth *Agrius convolvuli* using a needle electrode.

At rest, a distribution of P_{O_2} corresponding to levels in the muscle and tracheal structures was observed. At the onset of tethered flight, P_{O_2} in the muscle decreased. However, during a long stable flight, P_{O_2} increased and reached a plateau approximately 2 min after the onset of flight. During stable tethered flight, P_{O_2} in the centre of the second layer of the dorsal longitudinal muscle was locally higher than that during rest. As wing amplitude increased, P_{O_2} increased in spite of the concurrent increase in metabolic rate. During tethered flight at a constant wing amplitude, P_{O_2} was proportional to the mean wing positional angle.

The results suggest that this insect effectively uses muscle movement, which increases the frequency and stroke volume of ventilation, to augment gas exchange during flight.

Key words: oxygen microelectrode, gas transport, insect, hawkmoth, *Agrius convolvuli*, flight, metabolic rate.

Introduction

The wing muscle of a flying insect is the most active tissue known (Weis-Fogh, 1964). Aerobic metabolism in this muscle is supplied with oxygen by the trachea, an organ of intricate geometry but simple structure. The gas transport system in a flying insect differs drastically from that in a mammal in that an insect has no respiratory pigment to carry oxygen to the tissues and no diaphragm to drive expiratory/inspiratory gas flow (Schmidt-Nielsen, 1990; Mill, 1985). The insect tracheal system conveys oxygen from the atmosphere directly to the tissues and conveys carbon dioxide in the reverse direction. A tracheal system consists of air-filled tubes with the open ends connected to the atmosphere by spiracles and the closed ends penetrating the surrounding tissue as tracheoles. The tracheoles taper to less than 1 μm in diameter, enabling them to supply oxygen directly to each muscle fibre. This means that, for moderately sized insects, diffusive gas transport alone can sustain the resting metabolic rate, but that convective transport is required during flight. Large insects such as the giant belostomid bug *Lethocerus uhleri* also require convective transport at rest (Weis-Fogh, 1967), whereas small insects such as the mosquito do not require convective transport during flight. Two mechanisms by which insects create a flow of air in the tracheae are known. These are (1) by abdominal or thoracic pumping and (2) by movements of the surrounding muscles (muscle pumping). Some insects have large air sacs and muscles for ventilation. The muscles compress and expand the abdominal segments or deform the thoracic cuticle and thus compress the air sacs. For example, a honeybee ventilates by abdominal movement, especially during and after flight (Snodgrass, 1984). Such ventilation behaviour produces a unidirectional flow in the tracheae of large stroke volume. The second mechanism is muscle pumping. Weis-Fogh (1967) suggested that muscle contractions during flight led to changes in the total volume of the tracheae, thereby producing high-frequency oscillatory ventilation with a small tidal volume (Fig. 1). Weis-Fogh (1967) showed that ventilation caused by such muscle pumping is adequate for supplying oxygen in the locust *Schistocerca gregaria* during flight. He measured both the change in thoracic volume caused by the wing movements of the locust *S. gregaria* (25 μm per stroke) and the difference in oxygen concentration between the expired air (air sacs) and inspired atmospheric air (7.1 %). However, the details of gas transport inside a flying insect, especially at the distal end of the tracheoles, are unknown. In the present study, the oxygen partial pressure (P_{O_2}) in a wing muscle of the hawkmoth *Agrius convolvuli* was measured directly using a needle electrode, and the relationship between P_{O_2} and flight activity was investigated.

Materials and methods

Pupae of laboratory-reared sweet potato hawkmoths, *Agrius convolvuli* (L.), were supplied by the National Institute of Sericultural and Entomological Science (Kiguchi and

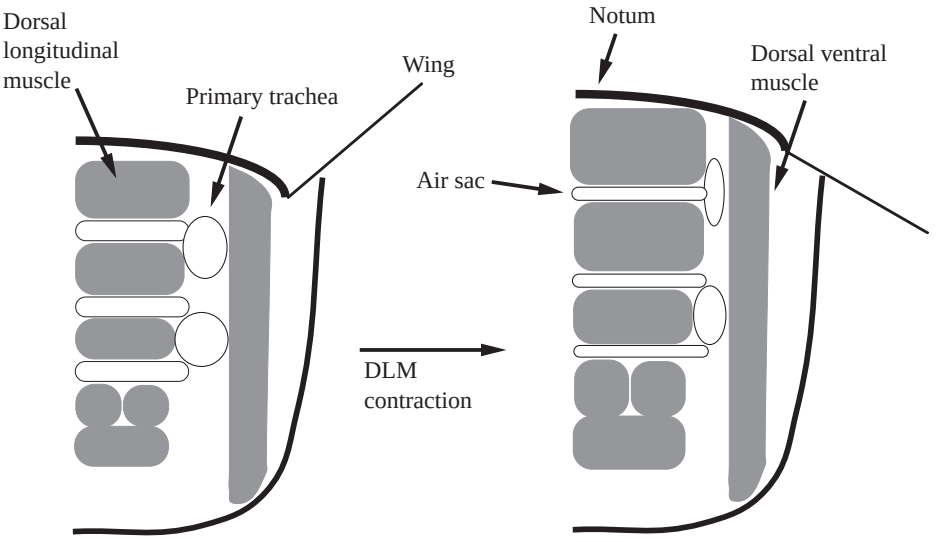

Fig. 1. Mechanism of tracheal deformation during muscle contraction. Contraction of the dorsal longitudinal muscle (DLM) raises the notum, and this elevates the wing base, causing the wing tip to depress. The contracted, thickened DLM deforms the tracheae, inducing air flow within them.

Shimoda, 1994). Adult moths, 3–5 days old, were used for experiments (N=100).

Moths were tethered to the experimental apparatus shown in Fig. 2A. To avoid damaging the moth, it was anaesthetized using carbon dioxide during the tethering procedure. The hairs on the thoracic tergites were removed, and the moth was attached using adhesive to a small plate attached to a rigid rod. Moths were then allowed to recover for 5–10 min in normal air. Measurements were started at least 1 h after the moth had regained the ability to beat its wings in a natural motion. The rod was mounted on a manipulator so that the position of the moth could be adjusted to be viewed through a microscope. A piece of thoracic cuticle (approximately 1 mm×2 mm) was removed to expose the underlying muscle so that an oxygen microelectrode (see below) could be inserted. This was connected to a picoammeter for measurement of P_{O_2}. The position of the electrode was controlled by a piezo manipulator with an infrared displacement meter to an accuracy of 1 μm. During insertion of the electrode, deformation of the muscle was minimized by moving the electrode back and forth (usually 30 μm forwards and 10 μm backwards). Thoracic temperature was measured using a type T thermocouple (50 μm in diameter) inserted into the contralateral muscle. The junction of the thermocouple was electrically sealed using acrylic resin. Temperature and P_{O_2} measurements were recorded simultaneously. During the tethered-flight experiments, an air flow of 2–4 m s^{-1} was produced by a direct current fan. Wind temperature was monitored using a platinum thermometer, and opening/closing of the wings was monitored using a photosensor attached to a voltmeter. All outputs were connected to a personal computer *via* a general purpose interface bus (GPIB). The moth was video-taped at 60 fields s^{-1} during the experiment using a miniature charged coupled device (CCD) camera positioned in front of the moth. The position of the edge of the right forewing was digitized from the video tape at every field and used to calculate the variation over time of the wing stroke amplitude and the wing positional angle.

Oxygen microelectrode

Details of the oxygen electrode are shown in Fig. 2B. The electrode reduces dissolved oxygen on the platinum cathode as follows:

$$\text{Cathode (Pt):}\quad O_2 + 2H_2O + 4e^- \rightarrow 4OH^-, \qquad (1)$$

$$\text{Anode (Ag):}\quad 4Ag + 4Cl^- \rightarrow 4AgCl + 4e^-. \qquad (2)$$

In an optimum range of reduction potential, all oxygen molecules reaching the cathode are reduced so that the reduction current is determined by the oxygen flux towards the cathode (limiting diffusion current). The oxygen flux is proportional to the difference in oxygen partial pressure between the cathode and a position just outside the recess in the tip of the electrode (Fig. 2B). Because the oxygen partial pressure is zero at the cathode, the reduction current is proportional to the oxygen partial pressure at a position just outside the tip recess. To obtain an optimum reduction potential, the reduction current was recorded at different levels of reduction potential in hawkmoth muscle tissue. A plateau was reached at approximately −0.6 V, which corresponds to the limiting diffusion current. The electrode was therefore operated at a reduction potential of −0.6 V, which is termed the reduction potential of oxygen.

To convert the recorded current to the oxygen partial pressure, the electrode was calibrated at five different oxygen partial pressures for each measurement. The electrode was calibrated in Theorel buffer (Baumgärtl, 1987) equilibrated by bubbling with gas mixtures of oxygen (0–20 %) and nitrogen (100–80 %), and thermally regulated at 30 °C. The oxygen concentration and the temperature were controlled within 0.1 % and 0.2 °C, respectively. The reduction current at 20 % oxygen ranged from 200 pA to 2 nA. The sensitivity of the electrode depends mainly upon the tip geometry. Calibration was carried out four times: twice before a measurement, once immediately after a measurement, and once after the electrode had been cleaned using an ultrasonic cleaner. The mean correlation coefficient between the reduction current and the

oxygen partial pressure was 0.9993 over 228 calibrations. The response of the electrode showed good linearity, and the regression curve agreed with the measured reduction current within 5 %.

In preliminary experiments, the stability of the electrode was also examined by inserting it into the muscle of a hawkmoth anaesthetized using chloroform vapour. The reduction current decreased by 10–20 % due to contamination by the tissue; therefore, the conversion from reduction current to oxygen partial pressure was carried out using the calibration curve recorded immediately after a measurement. Stable output signals were recorded, except for the initial decrease in the first 5 min or so after inserting the electrode. This initial decrease may have been caused by contamination of the electrode surface, increasing the diffusion layer and thus decreasing the reduction current. To avoid this initial decrease, measurements were begun 10 min after inserting the electrode. Taking into account the memory storage on the picoammeter and the response time of the electrode, a sampling frequency of 10 Hz was chosen.

Experimental procedures

In rest experiments, 30 animals were investigated to obtain the profile of P_{O_2} in the flight muscle. Moths were paralyzed by injection of 0.2 ml of 10^{-5} mol l^{-1} tetrodotoxin into the haemolymph approximately 10 min before the measurement. The electrode was inserted 300 μm into the muscle, and the signal from the electrode was allowed to stabilize; it was then moved forward to 2440 μm depth in steps of 20 μm. P_{O_2} was measured for 40 s at each depth (108 points). Only one insertion was made in each animal.

Forty animals were used in flight experiments. Experiments were limited to 2 h, owing to muscle damage and to fatigue of the hawkmoth. Again, only one insertion was made per animal. Measurement was started when the output from the electrode had stabilized after insertion into the muscle. The electrode was inserted into the dorsal longitudinal muscle (DLM) at four different depths (for 30 min each): 500, 1000, 1500 and 2000 μm, and P_{O_2} variation during flight was recorded twice at each depth. Flight was initiated and maintained by wind stimuli of 2–4 m s^{-1}. Mechanical stimuli (touching the legs of the moth with a needle) were used only when the moth did not start beating its wings spontaneously. The moth usually stopped beating its wings 2–4 min after the onset of flight, and the fan was then turned off. Otherwise, the fan was turned off to end the flight.

Determination of electrode position

The path of the inserted electrode was determined using a three-dimensional inner structure microscope (3DISM) (Kudoh *et al.* 1994) after the P_{O_2} and temperature measurements had been completed. The thorax was isolated and immersed in a mixture (1:1) of water and embedding agents (OCT compound) for a cryostat microtome, under low pressure (almost saturated with water vapour) for 1 day. The sample was then transferred to the pure embedding agent and frozen at −25 °C in a freezer. A microslicer was used to slice off the serial uppermost 30 μm thick layers, exposing the underlying sections. Sequential images of these exposed top surfaces were then examined using a binocular microscope and recorded using a laser video recorder (Sony LVR-8500). The thorax was reconstructed digitally from these images (Silicon Graphics, AVS) to determine the path of the electrode. Muscle damaged by the insertion of the electrode was darker in colour,

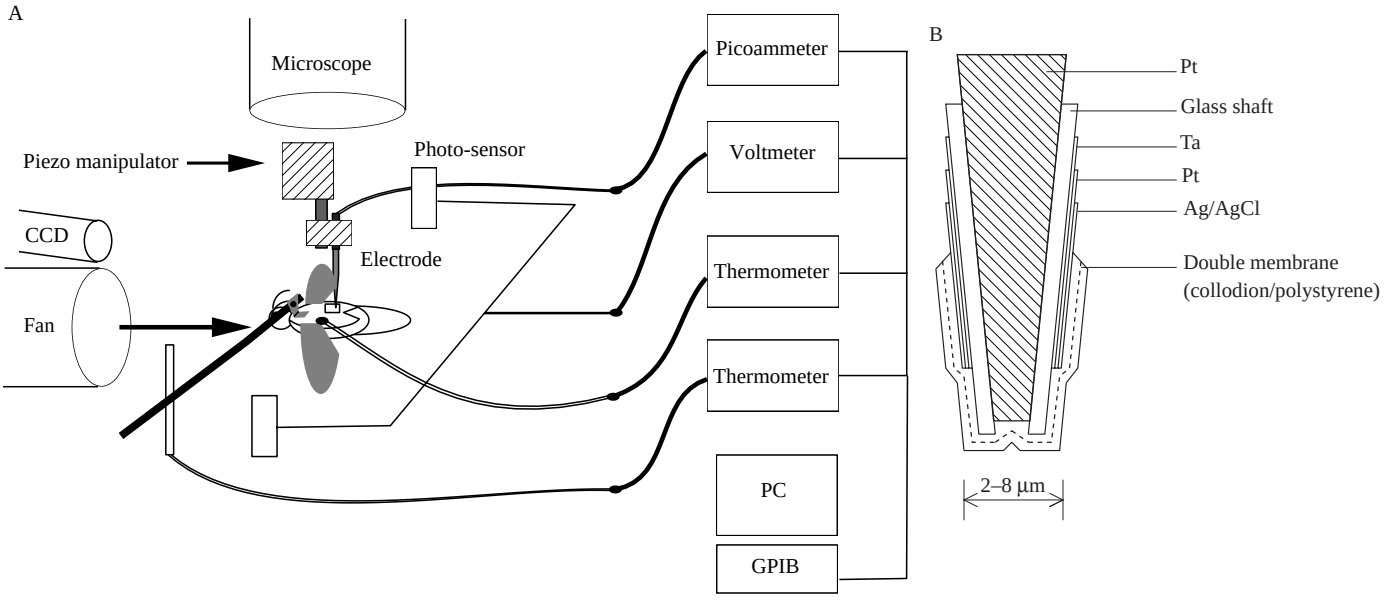

Fig. 2. (A) Experimental arrangement used to record P_{O_2} and muscle temperature from the flight muscles of a tethered sweet potato hawkmoth *Agrius convolvuli*. For further details, see text. (B) Polarographic microcoaxial electrode (Pt–Ag/AgCl, −0.6 V) with a 2–8 μm tip diameter used to measure P_{O_2}.

making the path easy to determine from the images without additional staining.

Anatomical study

Geometrical information about the thorax was obtained from frozen sections (N=20) and dissections (N=10). The procedure for freezing thoraces was the same as for 3DISM except for the time allowed for degassing the tracheae (1–2 h under low pressure). Hairs were removed before the thorax was isolated. Several methods were used to fix the thoracic muscle; freezing the muscle within 2–3 h after isolation to keep it fresh was found to be the best method of reducing deformation of the sectioned thorax. The frozen material was sectioned using a cryostat microtome (Microtome HM 500-OM), with a box temperature of −12 °C and with the material at −20 °C. The sections were 16–22 μm thick for observations of the whole thorax and 6–10 μm thick for observations of the tracheae and tracheoles. The sections were observed using a light microscope (Edge Scientific R440) without staining. The dissection was performed after fixation in 4 % neutral buffered formaldehyde for 2 weeks.

Results

One of the known problems of using polarographic electrodes is the existence of temperature effects. In the present experiments, changes in muscle temperature may cause errors in estimating P_{O_2}. The effects of temperature on the electrode were evaluated in Theorel buffer (Fig. 3). The sensitivity of the electrode increased linearly with solution temperature. A muscle temperature change from 30 to 35 °C, for example, will produce a calibration error of 14 % if the effect of temperature is neglected. For this reason, P_{O_2} values were corrected using muscle temperature data and a linear regression acquired from the data shown in Fig. 3. A second possible problem is the leakage of oxygen along the electrode barrel. To check the oxygen flux from the hole in the thoracic cuticle to the site of measurement, droplets of either Ringer's solution (Hoyle) or glycerine were placed onto the dissected region to seal the hole, and P_{O_2} in the muscle was monitored. In this experiment, P_{O_2} did not change below the droplet from a depth of 300 μm to 2500 μm from the muscle surface. It was concluded that any effect of oxygen diffusing from the exposed muscle surface was negligible. Because Ringer's solution penetrates the muscle and impairs its function, this treatment was not used in the main experiments.

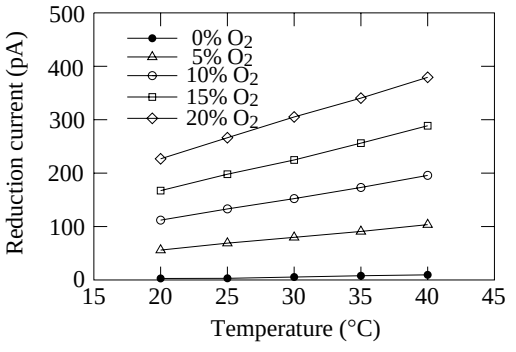

Fig. 3. Effect of temperature on electrode sensitivity. The electrode was calibrated in Theorel buffer at different temperatures and at different oxygen concentrations, C_{O_2}. Oxygen concentration (%) can be converted to oxygen partial pressure (P_{O_2}, kPa) using $P_{O_2}=(101-P_a)\times C_{O_2}$, where P_a is the saturated vapour pressure of water. The sensitivity increases linearly with temperature.

Structural features of the thoracic muscles and tracheae

The dorsal longitudinal muscle (DLM), a wing depressor, was studied in all experiments. Fig. 4 shows a side view of the DLM and the trachea supplying it. The DLMs consist of four layers (i–iv) in longitudinal section, the most ventral layer (iv) consisting of three parts (see also Fig. 6). A primary trachea approximately 400 μm in diameter led from a spiracle on the lateral surface of the thorax and ran parallel to the DLM surface. The distal end of the primary trachea entered the DLM between layers iii and iv. Neither an air sac nor an inflated portion of the trachea was visible in this region. Between the DLMs were dendroid bifurcations of the trachea (5–35 μm in diameter), and connected to these were thin air sacs that had no taenidia on the surface. The air sacs spread out between the branches. Most tracheae (20 μm in diameter) penetrating the muscles branched off from the air sacs. No air sacs were observed between sublayers in DLM layer iv. Near the plane of longitudinal symmetry of the thorax, a large number of bifurcated tracheae ran parallel to each other. Air sacs that could be compressed by nonflight muscles were not observed. This, together with the fact that abdominal or thoracic pumping was not observed during experiments, suggests that oxygen transport is carried out by diffusion

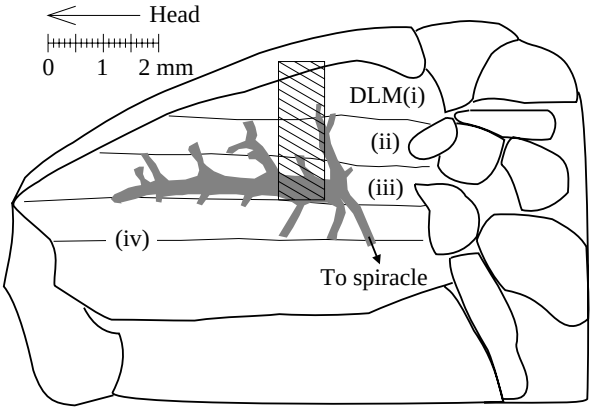

Fig. 4. The tracheal network supplying the dorsal longitudinal muscles (DLMs). This tracing from a micrograph shows a side view of the thorax after removal of the lateral cuticle and the dorsal ventral muscles. For simplicity, the bifurcated branches of the tracheae that were not connected to the DLMs are not shown. The hatched portion corresponds to the region in which the electrodes were placed. The trachea is shown shaded. The four layers of the DLM (i–iv) are shown. Layer iv could be subdivided into three parts (see also Fig. 6).

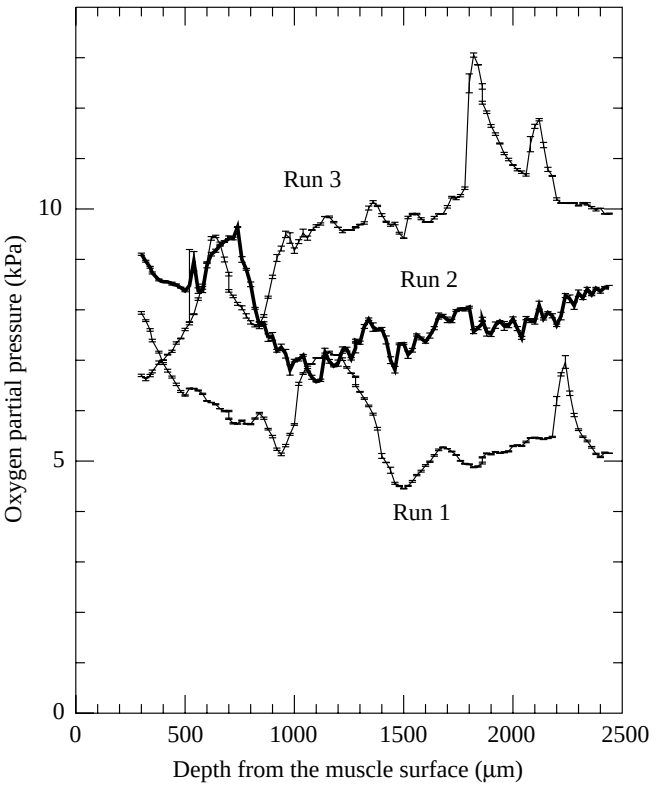

Fig. 5. Resting P_{O_2} profiles in the dorsal longitudinal muscle for three hawkmoths *Agrius convolvuli*. P_{O_2} profiles were acquired from moths paralyzed by injection of 0.2 ml of 10^{-5} mol l^{-1} tetrodotoxin into the haemolymph. P_{O_2} was measured every 20 μm from 300 μm to 2440 μm depth from muscle surface. Values were averaged over 20 s. Error bars show standard errors. These insertion paths are shown in Fig. 6.

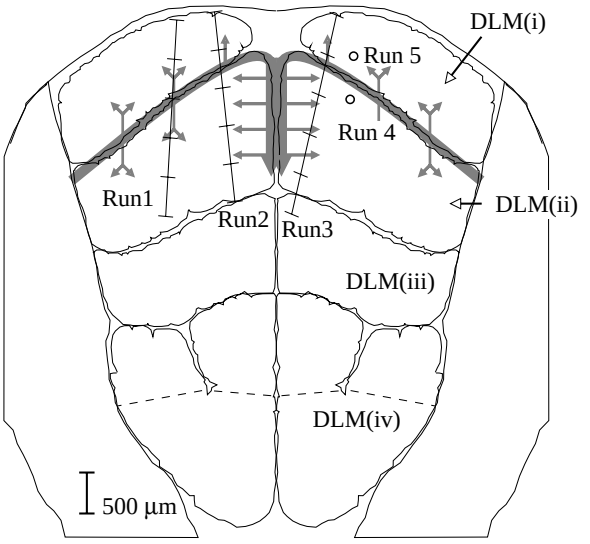

Fig. 6. Cross section through the thorax showing the paths of the electrode through the dorsal longitudinal muscles (DLMs). Runs 1–3 were carried out on resting (paralyzed) animals (see Fig. 5). A crossbar is marked at each 500 μm depth. The interval between crossbars differs for each run because the size of the thorax varied among individuals. The electrode positions in flying animals are indicated by circles (runs 4 and 5). The four layers of the DLM are labelled i–iv. Layer iv can be divided into three parts (broken line). The largest tracheae run between muscle layers (shaded). Arrows indicate the direction and path of oxygen transport.

alone at rest and as a result of flight muscle activity during flight.

Resting measurements

Three representative examples of the resting P_{O_2} profiles are shown in Fig. 5. At rest (following a 0.2 ml injection of 10^{-5} mol l^{-1} tetrodotoxin), P_{O_2} generally varied between 4 and 10 kPa as a function of depth from the surface of the DLM. The P_{O_2} profiles of both runs 1 and 2 shown in Fig. 5 initially decreased as depth increased and then increased to local maxima at depths of 1200 μm and 780 μm, respectively, after which P_{O_2} remained relatively constant with small fluctuations. The P_{O_2} of run 3 increased as the depth increased to 600 μm. Then, after a drop to a local minimum at 900 μm, it was relatively stable between 1000 μm and 1800 μm.

The precise paths of the electrode are shown in Fig. 6. The peaks in P_{O_2} in runs 1–3 (Fig. 5) correspond to when the electrode was positioned in the gap between DLM(i) and DLM(ii). Large tracheae (30 μm in diameter) and air sacs ran laterally through these gaps to the centre line of the body (Fig. 6). The surface of each muscle layer has the best supply of oxygen, whereas the centre of the each muscle layer is relatively oxygen-poor. The maxima and minima of the P_{O_2} profiles for runs 1 and 2 (Fig. 5) follow this pattern. In run 3, the region near the centre of the moth's body is supplied with oxygen from the trachea at the midline, resulting in a relatively constant oxygen level between a thoracic muscle depth of 1000 μm and 1800 μm. Sharp maxima, such as that at 2240 μm in run 1 (Fig. 5), may have been caused by the electrode puncturing a trachea in the DLM. The detailed geometry of the tracheal network was not determined for each experiment because of the operating resolution of the 3DISM (30 μm per pixel).

The P_{O_2} maximum was higher in run 3 than in runs 1 and 2. However, comparison among runs is complicated by the fact that insertion pathways differ. Although the insertion paths are represented on the same transverse section in Fig. 6, the actual paths were not on the same plane and were from different animals. P_{O_2} also depends on longitudinal position and body size. Profiles similar to those shown in Fig. 5 were obtained in other individuals, although slight changes to the insertion path caused quantitative changes in the P_{O_2} profile.

Flight measurement

When the moth was in flight, P_{O_2} in the muscle changed as a function of time, flapping intensity and wing position. Fig. 7 shows representative patterns. Initially, P_{O_2} in the muscle decreased from 10.83 to 7.60 kPa over the first 4 s, then recovered gradually to almost the resting level (mean P_{O_2} at 10 s is 8.57 kPa). This pattern of variation in P_{O_2} was observed

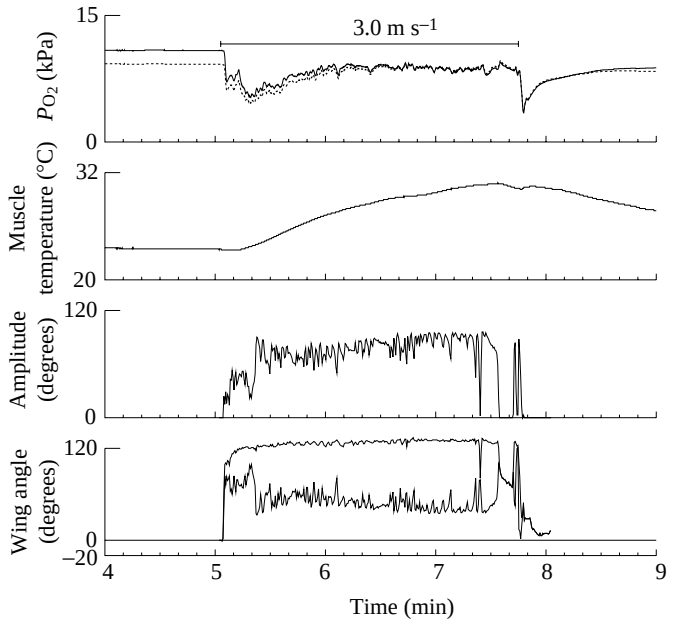

Fig. 7. P_{O_2}, muscle temperature, wing stroke amplitude and wing positional angle during flight in a hawkmoth *Agrius convolvuli*. Data are for run 4 at a microelectrode depth of 1000 μm (see Fig. 6). In the top panel, solid and broken lines show P_{O_2} calculated from the reduction current recorded with and without taking the muscle temperature change into account, respectively. The horizontal bar indicates the duration of the wind stimulus (3.0 m s^{-1}). The second panel shows muscle temperature. Wing stroke amplitude was measured from video recordings, and the amplitude of the right forewing, averaged over six wing strokes (=200 ms), is plotted. In the bottom panel, the minimum and maximum positional angles of the wing are plotted. Values were averaged over six wing strokes of the right forewing.

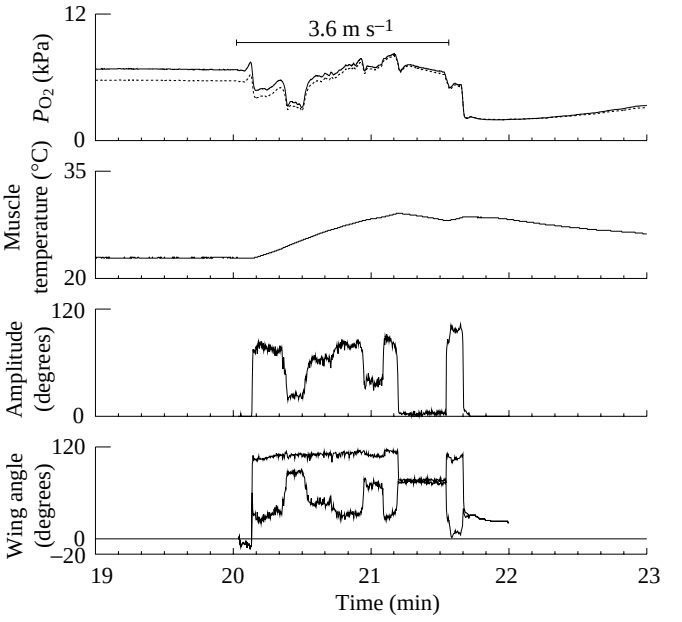

Fig. 8. Similar recordings to those shown in Fig. 7 for a different experiment (run 5, microelectrode depth 500 μm; see Fig. 6) showing the relationship between P_{O_2} and wing stroke amplitude. Details are as in Fig. 7. To vary the wing stroke amplitude, a thin plate was placed intermittently in front of the fan to interrupt the wind. Changes in wing stroke amplitude caused changes in P_{O_2}. When the amplitude exceeded 5 °, similar to that in natural flight motion, the flapping frequency was stable at approximately 30 Hz.

most frequently in all individuals and indicated that gas transport was augmented as the rate of oxygen consumption increased from the resting level. P_{O_2} variation depended on the position in the DLM. Compared with a moth at rest before flight, a moth in stable long flight has a lower P_{O_2} at the centre of DLM(i) and a higher P_{O_2} at the centre of DLM(ii). Because P_{O_2} in a muscle is determined by the relationship between oxygen demand and oxygen supply, both muscle activity and gas transport activity are considered below.

Wing stroke amplitude and positional angle were taken as indices of activity. A representative pattern of P_{O_2} and wing stroke amplitude is shown in Fig. 8. Although it is likely that the rate of oxygen consumption increases with increasing wing amplitude as a result of an increase in muscle contraction, P_{O_2} increased in concert with wing amplitude, showing that the oxygen supply increased as the wing amplitude increased. The augmented oxygen supply is more than sufficient to meet the oxygen demand during flight. Although the wingbeat frequency and muscle temperature are important variables for oxygen demand, there was no observable relationship between the P_{O_2} and either wingbeat frequency or muscle temperature. Wingbeat frequency was determined from the video tapes, by counting the strokes manually each second, and did not change by more than 10 % from 30 Hz in observations lasting for 1 min (approximately 1800 strokes). The relationship between P_{O_2} and muscle temperature had a correlation coefficient ranging from –0.27 to 0.35 for all flights (P>0.05). The changes in P_{O_2} were not dependent on temperature changes (see Fig. 8) although, on occasions when both P_{O_2} and muscle temperature increased, they were exceptionally well correlated (e.g. r=0.94, P<0.05 from 5.5 min to 6.0 min in run 4; Fig. 7).

The variation in P_{O_2} was correlated with wing positional angle. It was observed that, during periods of constant wing beat amplitude, P_{O_2} increased with mean wing positional angle (the average of maximum and minimum positions). In a typical case, P_{O_2} increased from 6.27 to 10.10 kPa as the mean positional angle changed from 57.0 to 80.9 ° at a constant amplitude of 48.6 ° (r=0.87, P<0.05).

The change in P_{O_2} per degree change in the mean positional angle was 0.22–0.29 kPa degree^{-1} for three runs. This relationship between P_{O_2} and the mean positional angle can be understood by considering the gas transport mechanism of the hawkmoth. The hawkmoth has no air sacs of large volume to contribute to ventilation; it is changes in the shape of the trachea itself that drive oscillatory air flow during flight muscle contraction. Examination of tracheal structure using a light microscope shows that a transverse section of a trachea

is circular or elliptical with an aspect ratio of near unity when the muscle is relaxed. When the muscle is contracted, the transverse section becomes a more collapsed ellipse (see Fig. 1). The DLM of the hawkmoth is a wing depressor muscle; it is contracted as the wing is depressed. In this type of ventilation system, air flow induced by muscle contraction is a function of mean wing positional angle. Furthermore, the gas transport efficiency deteriorates in a narrow tube, and because the trachea is a tube and is almost collapsed when the mean wing positional angle is low, the gas transport efficiency is reduced.

Discussion

During steady flight, there was an increase in the efficiency of gas transport (increased P_{O_2} in the DLM) which presumably corresponded with muscle activity (metabolic rate) during flight. The difference between the partial pressures of oxygen in atmospheric air and in a muscle is the driving force for convective/diffusive oxygen transport, and the efficiency of oxygen transport is evaluated from the metabolic rate divided by this driving force. In a variety of insects, the rate of oxygen consumption was found to range from 0.01 to $0.04\,\mathrm{ml\,O_2\,g^{-1}\,muscle\,min^{-1}}$ at rest and increased 50–400 times during flight (Weis-Fogh, 1964). Bartholomew and Casey (1978) showed that the body-mass-specific metabolic rate during hovering flight in moths was approximately 148 times higher than that during rest and was only slightly dependent on body mass.

To investigate the mechanism of gas transport in a hawkmoth during flight, the size of the tracheae and the fluid parameters were examined (see Appendix). Examination of tracheal structure using a light microscope suggests that the large tracheae and air sacs can be compressed by muscle contraction, thereby inducing flow in the tracheal network. A hawkmoth has no diaphragm to drive the exchange all the gas in the tracheal network with fresh air during one contraction, and it is unlikely that all the tracheae can be collapsed completely to flush out all the gas inside the body. This incomplete exchange suggests that inspired atmospheric air will not reach the muscle fibres, but will be expired again during the expiration phase. Birds have a unidirectional ventilation flow through their respiration system; the air flows through the main bronchus to the caudal sacs during inspiration, and the air from the caudal sacs flows through the lung during expiration (Schmidt-Nielsen, 1990). Although certain large insects, such as the locust *Schistocera gregaria* (Weis-Fogh, 1964), have a shunt mechanism in the primary trachea, the hawkmoth does not. It does not use unidirectional ventilation flow, and it is not known whether other large insects use unidirectional flow.

High-frequency ventilation of a small tidal volume can significantly enhance fluid mass transport (Drazen *et al.* 1984). However, the fluid variables in a hawkmoth differ greatly from those found in known mechanisms such as Taylor dispersion (Watson, 1983) and steady streaming (Hydon and Pedley, 1993). In Taylor dispersion, a radial velocity gradient augments axial mass transport. The expected augmentation by this mechanism in the hawkmoth estimated using the theoretically derived equation of Watson (1983) is only 3 % greater than for molecular diffusion. Gas transport augmentation can also occur by steady streaming due to asymmetry between the inspiration and expiration flow profiles. A well-known example of such transport is oscillatory flow through a tapering channel. The channel geometry flattens the flow profile of the inspired flow, whereas, because a tapering tube becomes an expanding tube during the expiration phase, the expiratory flow is greater at the centre of the channel (compared with a parabolic profile in a straight tube). Therefore, the averaged flow during one cycle is not zero; expiratory flow occurs at the centre of the tube and inspiratory flow near the wall. This bi-directional flow could thus supply oxygen and remove carbon dioxide even within a single tube.

Such bi-directional flow may occur in the large trachea of a hawkmoth; however, the known mechanisms which result in steady streaming are not sufficient: the fluid variables in a hawkmoth (see Appendix) are too small for these mechanisms to function. When the Reynolds number (*Re*) is approximately 1 and the frequency parameter α is approximately 1, flow profiles do not deviate from the normal parabolic profile (Poiseuille flow), even during streaming through a geometrically complicated channel.

Thus, in the hawkmoth, augmented gas transport occurs largely because the tracheal network itself is not only a channel but also a pump, whose cross-sectional geometry changes continuously during a ventilation cycle. The low values of *Re* and α mean that the velocity profiles must be like those of Poiseuille flow in an elliptical tube. However, changes in aspect ratio may produce non-zero averaged flow which, in turn, will enhance mass transport. Currently, there are no data on mass transport in channels that have cyclically changing cross-sectional areas.

The mechanism of air flow in the hawkmoth during flight remains unresolved. To increase oxygen supply to the muscle, the moth must increase its oxygen intake by increased flux not only through its large trachea but also through its fine distal tracheae. The use of convective transport in fine tracheae is more difficult because *Re* and α are significantly smaller than those in a large trachea. In addition, it is not known whether such small channels (1–20 μm in diameter) can be deformed by muscle contraction to cause an air flow. If the metabolic rate in the muscle increases by a factor of 100 during flight, there also needs to be a mechanism to increase oxygen flux through the fine tracheae.

Appendix

Fluid parameters in a trachea are evaluated as follows. Geometric information was obtained from micrographs of dissected hawkmoths and from frozen sections. The primary

trachea had a maximum diameter, D, of approximately 400 μm and a length, L, of 4.5 mm. The frequency parameter α in the primary trachea was calculated as 0.71 from D, the wingbeat frequency f (=30 Hz) and the kinematic viscosity of air ν (=0.15 $cm^2 s^{-1}$), where:

$$\alpha = \frac{D}{2}\sqrt{\frac{2\pi f}{\nu}}. \quad (3)$$

If we approximate the trachea as a cylinder, then the tracheal volume from the spiracle to the DLM, V_t, can be estimated as 5.6×10^{-4} cm^3 from the equation:

$$V_t = \pi\left(\frac{D}{2}\right)^2 L\ . \quad (4)$$

The diameter d of the trachea between the layers of the DLMs was 5–35 μm, and the longitudinal length l of a DLM was 1.0 cm. If the air sacs can expand to fill the three gaps between the muscle layers completely, then the total volume of the tracheal network between the muscles, V_a, can be evaluated as a trapezoidal prism whose bases b_a and b_b are 0.3 cm and 0.4 cm, respectively, where:

$$V_a = \frac{b_a + b_b}{2}\times l \times d \times 3. \quad (5)$$

giving a value of 3.6×10^{-3} cm^3. When direct ventilation does not occur, the ventilation stroke volume is less than the volume of the primary trachea, V_t, and the amplitude of the averaged velocity, U, is then:

$$U < \frac{V_t \times f}{2} \Big/ \pi\left(\frac{D}{2}\right)^2 = \frac{Lf}{2}\ . \quad (6)$$

Using the values given above, U<6.75 cm s^{-1}. During flight, the Reynolds number, Re, in the primary trachea is:

$$Re < \frac{DU}{2\nu}\ . \quad (7)$$

Therefore, Re<0.9.

I thank M. Shimoda and K. Kiguchi for hawkmoth pupae, H. Baumgärtl for technical advice on producing and handling an oxygen microelectrode, and H. Yokota, K. Kudoh and T. Higuchi for collaboration with 3DISM. The electrode was produced in collaboration with K. Tanishita and K. Oka at Keio University.

References

BARTHOLOMEW, G. A. AND CASEY, T. M. (1978). Oxygen consumption of moths during rest, pre-flight warm-up and flight in relation to body size and wing morphology. *J. exp. Biol.* **76**, 11–25.

BAUMGÄRTL, H. (1987). Systematic investigations of needle electrode properties in polarographic measurements of local tissue P_{O_2}. In *Clinical Oxygen Pressure Measurement* (ed. A. M. Ehrly, J. Hauss and R. Huch), pp. 17–42. London: Springer-Verlag.

DRAZEN, J. M., KAMM, R. D. AND SLUTSKY, A. S. (1984). High-frequency ventilation. *Physiol. Rev.* **64**, 505–543.

HYDON, P. E. AND PEDLEY, T. J. (1993). Axial dispersion in a channel with oscillating walls. *J. Fluid Mech.* **249**, 535–555.

KIGUCHI, K. AND SHIMODA, M. (1994). The sweet potato hornworm, *Agrius convolvuli*, as a new experimental insect: continuous rearing using artificial diets. *Zool. Sci.* **11**, 143–147.

KUDOH, K., YOKOTA, H. AND HIGUCHI, T. (1994). Development of microslicer implementation of 3-dimensional internal structure microscope. *Microoptics News optic Soc. Jap.* **12**, 59–64.

MILL, P. J. (1985). *Comprehensive Insect Physiology Biochemistry and Pharmacology*, vol. 3, *Integument, Respiration and Circulation* (ed. G. A. Kerkut and L. I. Gilbert), pp. 517-593. Oxford: Pergamon Press.

SCHMIDT-NIELSEN, K. (1990). *Animal Physiology: Adaptation and Environment*, 4th edn, pp. 5–126. Cambridge: Cambridge University Press.

SNODGRASS, R. E. (1984). *Anatomy of the Honey Bee*, pp. 134–167, 227–242. Ithaca, London: Comstock Publishing Associates.

WATSON, E. J. (1983). Diffusion in oscillatory pipe flow. *J. Fluid Mech.* **133**, 233–244.

WEIS-FOGH, T. (1964). Diffusion in insect wing muscle, the most active tissue known. *J. exp. Biol.* **41**, 229–256.

WEIS-FOGH, T. (1967). Respiration and tracheal ventilation in locusts and other flying insects. *J. exp. Biol.* **47**, 561–587.